Addressing wellbore integrity and thief zone permeability using microbially-induced calcium carbonate precipitation (MICP): A field demonstration

Catherine M. Kirkland, Abby Thane, Randy Hiebert, Robert Hyatt, Jim Kirksey, Alfred B. Cunningham, Robin Gerlach, Lee Spangler, Adrienne J. Phillips

Kirkland, C. M., Thane, A., Hiebert, R., Hyatt, R., Kirksey, J., Cunningham, A. B., ... & Phillips, A. J. (2020). Addressing wellbore integrity and thief zone permeability using microbially-induced calcium carbonate precipitation (MICP): A field demonstration. Journal of Petroleum Science and Engineering, 190, 107060.

Addressing wellbore integrity and thief zone permeability using microbially-induced calcium carbonate precipitation (MICP): a field demonstration

Abstract

Microbially-induced calcium carbonate precipitation (MICP) is an emerging biotechnology for wellbore integrity applications including sealing defects in wellbore cement and modifying the permeability of rock formations. The goal of this field demonstration was to characterize a failed waterflood injection well and provide proof of principle that MICP can reduce permeability in the presence of oil using conventional oilfield fluid delivery methods. We compared well logs performed at the time the well was drilled with ultrasonic logs, sonic cement evaluation, and temperature logs conducted after the well failed. Analysis of these logs suggested that, rather than entering the target waterflood formation, injectate was traveling through defects in the well cement to a higher permeability sandstone layer above the target formation. *Sporosarcina pasteurii* cultures and urea-calcium media were delivered 2290 ft (698 m) below ground surface using a 3.75 gal (14.2 L) slickline dump bailer to promote mineralization in the undesired flow paths. By Day 6 and after 25 inoculum and 49 calcium media injections, the injectivity [gpm/psi] had decreased by approximately 70%. This demonstration shows that 1) common well logs can be used to identify scenarios where MICP can be employed to reduce system permeability, remediate leakage pathways, and improve waterflood efficiency, and 2) MICP can occur in the presence of hydrocarbons.

Keywords: Microbially-induced calcium carbonate precipitation, MICP, *Sporosarcina pasteurii,* ureolysis, wellbore integrity, waterflooding

1.0 Introduction

1.1 Waterflooding for secondary oil recovery

Oil and gas extraction wells are becoming increasingly common features of the landscape as hydrocarbon production expands from conventional sandstone reservoirs to unconventional reservoirs like shale and tight sand formations. In 2014, there were 1,039,000 producing oil and gas wells in the United States, compared to 735,000 in 2000 (Energy Information Administration, 2018). In conventional reservoirs and even under the best conditions, less than half of the original oil in place is typically extracted during primary production, the period when oil flows freely from the reservoir rock due to the high differential pressure between the formation and the wellbore (Udy *et al.*, 2017, Yuan *et al.*, 2018). As primary production declines, oil and gas producers may employ waterflooding to promote secondary recovery. Waterflooding involves injecting water or brine into the oil-bearing formation to displace and sweep out residual hydrocarbons while also restoring formation pressure. Spatial heterogeneities in the reservoir rock and differences in fluid viscosities, however, can lead to conformance problems during waterflooding including viscous fingering, preferential flow through more permeable rock, and channel flow in fractures in well cement or the formation rock (Feng *et al.*, 2013, Ahmed *et al.*, 2015, Kargozarfard *et al.*, 2019). This study focuses on

mitigating poor waterflood efficiency caused by defects in the wellbore cement. Cement defects can lead to compromised wellbore integrity.

1.2 Wellbore cement integrity

With the increase in hydrocarbon production, comes increased concern for maintaining high water quality in aquifers above hydrocarbon-bearing strata and preventing emission of fugitive gases to the atmosphere via leaky wellbores (Davies *et al.*, 2014). As the well provides a direct conduit between the subsurface reservoir and the atmosphere, establishing and maintaining zonal isolation between geologic strata is vitally important for both production and injection wells. A recent study found that up to 9% of active wells drilled since 2000 in Pennsylvania, USA, have compromised cement or issues with casing integrity (Ingraffea *et al.*, 2014). Moreover, waterflooding and fluid injection to improve oil recovery may exacerbate cement failure in aging wells (Wang *et al.*, 2014).

Properly constructed (and abandoned) wells employ an impervious cement sheath between the well casing and the formation to prevent upward migration of fluids and gases. However, the cement sheath can degrade over time under the influence of thermal, geo-mechanical, and chemical stresses (Wang *et al.*, 2014, Bai *et al.*, 2016, De Andrade *et al.*, 2016, Carroll *et al.*, 2017). Fluids can seep into fractures and channels in the cement or flow through micro-annuli between the casing and cement or between the cement and formation (Newell *et al.*, 2013, Davies *et al.*, 2014, Opedal *et al.*, 2014, Wang *et al.*, 2014, Haagsma *et al.*, 2017). Depending on the nature of the cement defect and the adjacent rock formation, the fluid can migrate up the wellbore or into other rock strata.

Repairing a leakage pathway or wellbore cement defect is non-trivial. Cement squeezes are commonly used to repair larger defects. Fine cements can be injected through perforations in the casing to seal apertures as small as 120 µm before the viscosity of the cement and required pumping pressures interfere (Clarke *et al.*, 1993, Phillips *et al.*, 2018). According to industry estimates, up to 50% of the time, fine cement injection is not successful at sealing the leakage pathway (Bagal *et al.*, 2016). Gels, resins, and epoxies can be used to repair smaller defects, on the order of 1-100 µm, though these technologies are in an early stage of technological development and are more expensive than fine cement (Todorovic *et al.*, 2016, Phillips *et al.*, 2018). A major challenge in remediating wellbore leakage is proper placement of the sealing material to provide a strong and stable seal over time.

1.3 Microbially-induced calcium carbonate precipitation (MICP)

Recent research has explored how microbial metabolic processes can be harnessed to produce bio-cement consisting of precipitated calcium carbonate. Many strains of bacteria found naturally in soil and groundwater are ureolytic, meaning they produce the urease enzyme which catalyzes the hydrolysis of urea, also called ureolysis (Ferris *et al.*, 2003). Ureolysis provides a source of nitrogen for the microbes, increases the solution pH and alkalinity, and produces carbonate ions. When there is also sufficient calcium to exceed saturation conditions, calcium carbonate ($CaCO_3$) precipitation can occur [Eqn, 1].

$$CO(NH_2)_2 + 2H_2O + Ca^{2+} \rightarrow 2NH_4^+ + CaCO_3\,(s) \qquad [1]$$

Sporosarcina pasteurii, the ureolytic bacterium used in this demonstration, attaches to rock and cement surfaces with extracellular polymeric substances (EPS), forming a biofilm (Fridjonsson *et al.*, 2011). $CaCO_3$ precipitation occurs in association with the microbial biofilm matrix due to the mass transfer limitations and localized chemical gradients within the hydrogel structure (Decho, 2010). Additionally, the biofilm is believed to provide nucleation sites for precipitation to initiate (Stocks-Fischer *et al.*, 1999, Oppenheimer-Shaanan *et al.*, 2016). With continued injection of fresh microbial cultures and mineralization-promoting fluids, the $CaCO_3$ mineral thickens, bridging pore throats and fractures, filling voids, and sealing flow pathways.

1.4 Previous field demonstrations of MICP

Microbially-induced calcium carbonate precipitation (MICP) is being researched as an emerging technology for subsurface engineering applications that include both sealing defects in wellbore cement (Phillips, A. J. *et al.*, 2013, Cunningham *et al.*, 2014, Phillips *et al.*, 2018) and modifying the permeability of rock formations for possible enhanced oil recovery applications (Ferris *et al.*, 1996, Phillips, Adrienne J. *et al.*, 2013, Wu *et al.*, 2017). Most research related to MICP has been conducted at the laboratory scale, though several studies of note have been performed at field scale. Fujita *et al.* (2008) stimulated native ureolytic microbes in a calcite-saturated aquifer to investigate the potential for co-precipitating radionuclides from contaminated groundwater (Fujita *et al.*, 2008). Burbank *et al.* (2011) observed increased resistance to liquefaction in saturated soil following stimulation of indigenous ureolytic microbes and infiltration of calcium chloride solution (Burbank *et al.*, 2011). Gomez *et al.* (2015) used surficial application of MICP to stabilize loose sands and reduce erosion at a mine site in Canada (Gomez *et al.*, 2015), and van Paassen *et al.* (2010) performed *in situ* seismic measurements during MICP bio-grouting in a 100 m^3 sand-filled test cell (van Paassen Leon *et al.*, 2010). Cuthbert *et al.* (2013) applied MICP to reduce transmissivity in a rock fracture 24 m below ground surface (bgs)(Cuthbert *et al.*, 2013). The first field demonstration in a wellbore environment successfully used MICP to seal a horizontal "pancake fracture" in tight sandstone at a depth of 1115 ft (340 m) bgs (Phillips *et al.*, 2016). A subsequent demonstration in the same well resulted in MICP sealing of compromised wellbore cement 1017 ft 310 m (310 m) bgs (Phillips *et al.*, 2018). To our knowledge, no field scale demonstrations of MICP have been performed in a working oil or gas well or in the presence of hydrocarbons prior to the current work.

1.5 The current study - overview

This field study was conducted in Indiana, USA, at a water injection well used for secondary oil recovery. Since the well had experienced a significant drop in waterflood efficiency, the goal of this field demonstration project was twofold: 1) to use available downhole characterization methods to develop a valid conceptual model of waterflood flow paths, and 2) provide proof-of-principle that MICP can significantly reduce system permeability in the presence of oil and using conventional oilfield fluid delivery methods. The well, located in Posey County, Indiana, had been used as a water injection well to sweep residual oil to production wells from 2010 – 2012 when injection pressure was lost, and the well was removed from service. We compared well logs performed at the time the well was drilled in 2006, including gamma ray, dual induction, and compensated density and neutron logs, with ultrasonic logs, sonic cement evaluation, and

temperature logs conducted after the well failed. Analysis of these logs suggested that, rather than entering the formation targeted for waterflood, injectate was traveling through defects in the well cement to a higher permeability sandstone layer above the target formation (Figure 1). Formations like this sandstone layer are also referred to as 'thief zones.' We applied MICP to validate its potential to address oil and gas wellbore integrity challenges. Microbial cultures and urea-calcium media were delivered using a 3.75 gal (14.2 L) slickline dump bailer to promote mineralization and reduce flow through the undesired flow paths. Progress in the field was assessed by monitoring the relationship between injection flowrate and pressure. The flow-to-pressure relationship describes the capacity of the system to receive fluids without fracturing the formation, also known as the system's injectivity. At the end of the demonstration, samples of mineral precipitate were collected from the injection tubing for bio-chemical analyses.

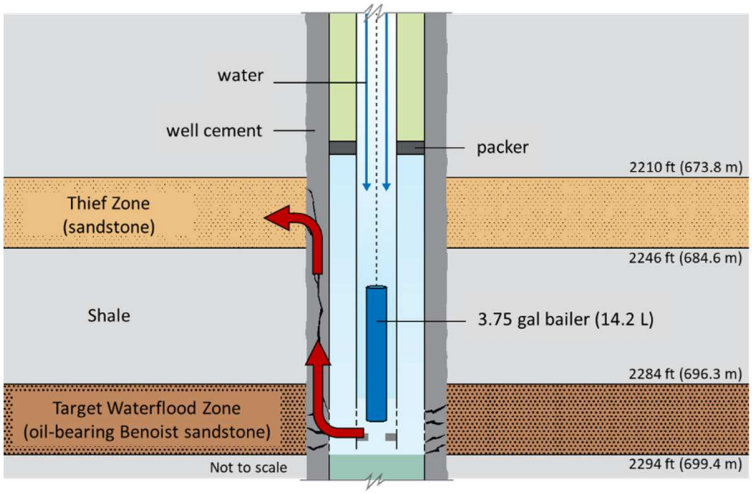

Figure 1. Conceptual model: a channel in the wellbore cement of the water injection well used for this field demonstration allowed injected fluids to travel to a more permeable sandstone layer 38-84 feet (10.4 – 25.6 m) above the target waterflood zone, which is a tight oil-bearing sandstone. Microbial cultures and urea-calcium media were delivered using a 3.75 gal (14.2 L) slickline dump bailer to promote mineralization and reduce flow through the undesired flow paths.

2. Materials and Methods

2.1 Site characterization

The subject well consists of a 7-7/8 inch (0.2 m) open hole drilled to 2540 ft (774.4 m) bgs. Gamma ray and dual induction logs (Figure 2), as well as compensated density and compensated neutron logs (not shown), were acquired prior to casing the well in 2006. These logs are typically used to identify the lithology and porosity of rock formations and differentiate between oil- and water-bearing strata. The logs showed tight oil-bearing Benoist sandstone between 2284 – 2294 ft (696.3 – 699.4 m) bgs, overlaid by shale up to approximately 2246 ft (684.6 m) bgs, and a higher permeability water-saturated sandstone between 2210 – 2246 ft (673.8 – 684.6 m) bgs. The well was fitted with a 5-1/2 inch (0.14 m) steel casing to a depth of 2319 ft (707 m) (bgs). The annulus between the open hole and the steel casing was filled with well cement and the well casing was perforated between 2284 – 2294 ft (673.8 – 684.6 m) bgs to access the oil-bearing Benoist sandstone.

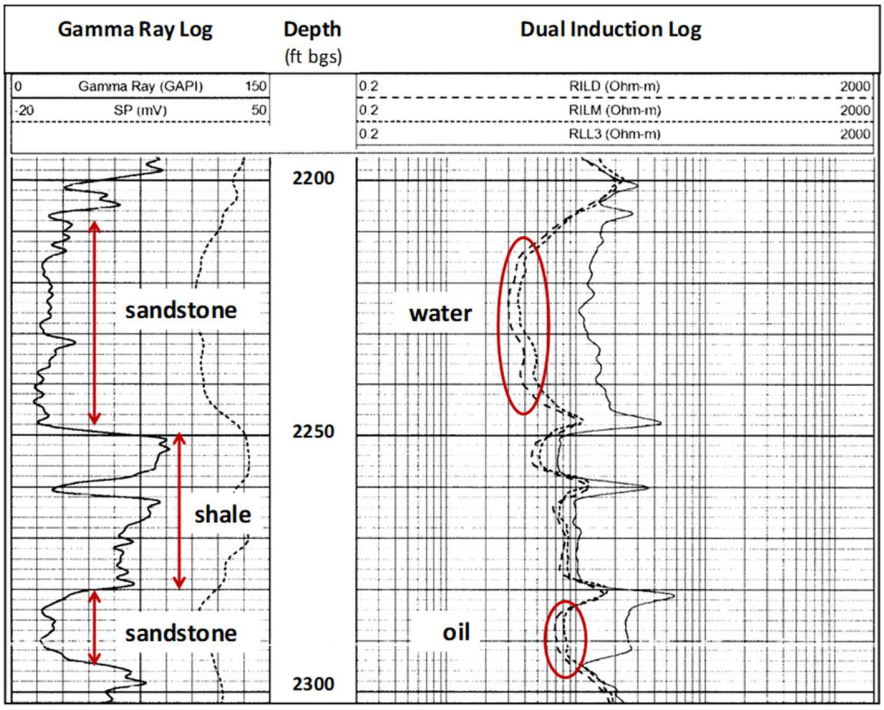

Figure 2. Gamma ray and dual induction logs completed in 2006 prior to casing the subject well identified an oil-bearing sandstone, overlaid by shale and a water-bearing sandstone.

Between 2010 - 2012, 966 barrels of water per month (BWPM) on average were injected at 1,400 – 1,500 psi (9.7 – 10.3 MPa), yielding 500 barrels of oil per month (BOPM) at a nearby producing well. In late 2012, injection pressure dropped to approximately 550 psi (3.8 MPa) and water injection increased to an average of 1,900 BWPM. Over the same period, oil production decreased to approximately 300 BOPM. The change in injectivity could have been caused by fracturing the Benoist sandstone with the high injection pressures or could indicate a failure of the wellbore cement.

To identify the cause of the change in injectivity, the well was evaluated with sonic and ultrasonic wellbore logging tools. These borehole tools can be used to image the condition of the casing and cement annulus by transmitting acoustic waves into the formation and receiving the attenuated, reflected waves at the detector. Changes in waveform amplitude arise from differing densities of material through which the acoustic or ultrasonic waves pass. Based on the waveforms detected, these tools can identify the presence of solids, liquids, or gases behind the casing via flexural attenuation of the acoustic impedance (SLG map, Schlumberger), detect leaks in the well casing, or evaluate the cement-to-casing and cement-to-formation bond (Johns *et al.*, 2009). A conventional sonic cement bond log (CBL) with variable density logging (VDL) can indicate whether there is unbonded pipe or a good cement bond (Frisch *et al.*, 1998) but cannot identify small channels within the cement annulus.

The SLG map produced from an ultrasonic Isolation Scanner (IBC) log showed the presence of good cement bonding above the elevation where a packer was previously set at 2,218 ft (676.2 m) bgs (Figure 3). Below this depth and including the location of the perforations used for waterflooding, there were no valid waveforms detected with the tool, likely due to heavily corroded casing. The CBL-VDL log was collected with a different tool string and was

less influenced by the condition of the casing. The CBL-VDL appears to suggest that good cement may extend to approximately 2245 ft (684.5 m) bgs as indicated by the wavy lines of the VDL (Figure 3). Parallel vertical lines indicate low signal attenuation due to poor cement bonding. No acoustic data, sonic or ultrasonic, were collected in the immediate vicinity of the perforations due to the presence of a bridge plug below the perforations.

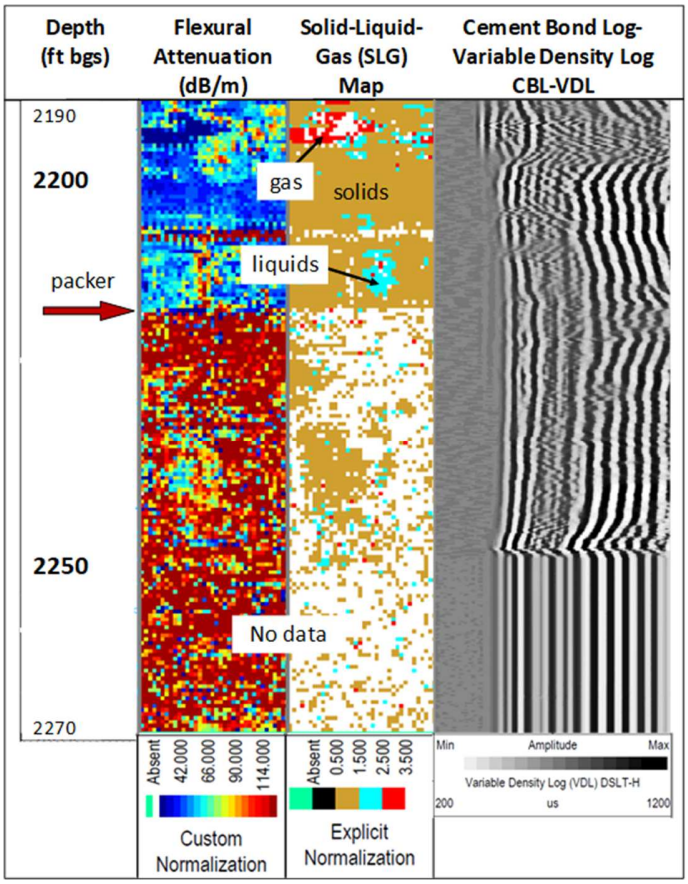

Figure 3. Sonic and ultrasonic well logging data collected to characterize well and identify cause of change in injectivity. The packer had been previously set at 2,218 ft (676.2 m) bgs (arrow) and well-bonded cement was observed above this elevation, shown as tan in the SLG map and in blue on the flexural attenuation log. Below 2,218 ft (676.2 m) bgs, corrosion of the casing prevented collection of useful data with the ultrasonic tool. The CBL-VDL appears to show good cement bonding to a depth of approximately 2245 ft (684.5 m) bgs, as indicated by the wavy lines of the VDL. Perforations for water flood injection are located 2284 – 2294 ft (696.3 – 699.4 m) bgs below the bottom of the well logs shown.

Since these well logs provided little information regarding the zone of interest, a wellbore temperature log was collected. Temperature logs can detect deviations from the reference temperature gradient in the well related to fluids of a different temperature entering or exiting the borehole (Loeb *et al.*, May, 1965). Cool fluids are injected into the well and the temperature logging tool is passed through the wellbore zone of interest periodically, monitoring the change in temperature as the strata warm the well casing and fluids toward equilibrium. The measurement is sensitive to temperature anomalies in the region just outside the well casing

and can be used to detect fluid flow through wellbore cement defects. Thus, the log was able to identify which failure scenario – fractured formation or failed cement - was more likely. The temperature log positively identified fluid travelling from the perforations along the outside of the casing in failed cement to an elevation of approximately 2230 ft (679.9 m) bgs. The temperature log appears later in the paper as Figure 5. Correlating the temperature log data to the original well logs collected in 2006 suggests that the well cement failed, possibly due to elevated injection pressures, up to an elevation where the formation transitioned from relatively impermeable shale to higher permeability sandstone thief zone above 2245 ft (684.5 m) bgs. As the injected water dispersed through the thief zone matrix, pressure on the wellbore cement and the volume of flow through it likely decreased. Certainly, above 2218 ft (676.2 m) bgs the cement provided a strong seal against upward fluid migration when the acoustic logs were collected.

In summary, based on knowledge of the lithology from the 2006 well logs, sparse information regarding cement condition from the acoustic logs, and evidence of flow through the cement annulus from the temperature log, the conceptual model shown in Figure 1 was developed and was used to design the injection strategies applied during the field demonstration. Pressure and flow data collected at the same time as the temperature log were used to estimate the aperture of the cement fracture. Assuming the flow passed through a single channel in the well cement and applying the cubic law (Zimmerman *et al.*, 1996) which describes a fluid's hydraulic behavior in a fracture, the aperture in the well cement was estimated to be approximately 400 µm at the narrowest point. MICP has been used to seal cement defects of similar dimensions in a laboratory study (Kirkland *et al.*, 2019). Moreover, the rock matrix of the sandstone thief zone provides an appropriate environment for MICP to occur (Phillips *et al.*, 2016, Verba *et al.*, 2016) thereby reducing permeability of the thief zone and system at large.

2.2 MICP field demonstration design

Prior to the demonstration, the plastic-lined injection tubing and injection packer were removed from the well. A 2-7/8 inch (7.3 cm) tubing "work string" with a tension-set packer was deployed in the well. The packer was set between 2187 – 2194 ft bgs (666.8 – 668.9 m) to isolate the region of interest from the upper strata, and the tubing landed in the tubing head in preparation for the experiment. The well was flushed with approximately 700 gal (2650 L) of fresh water to establish an initial injection pressure and flow relationship. Microbial cultivation was underway in the mobile laboratory upon its arrival on-site.

The 2-7/8 inch (7.3 cm) tubing accommodated a 3.75 gal (14.2 L) dump bailer used to deliver the biomineralization-promoting fluids. The bailer was lowered down the well tubing by a slickline rig until impact on a collar stop located at 2288 ft bgs (697.6 m). The force of impact was intended to shear a pin on the bailer, opening a valve and releasing the fluids contained within. Water injected down the tubing flushed the biomineralization fluids out of the bailer through a perforated pup joint at 2285 – 2288 ft bgs (696.6 – 697.6 m) and out of perforations in the steel well casing. Once outside the well casing, the biomineralization fluids were assumed to follow the most hydraulically favorable path, i.e. through the fractured cement and into the thief zone sandstone where precipitation was desired. The duration of the bailer round trip was approximately 30 minutes.

2.3 Biomineralization-promoting media

Two types of fluids were injected into the well to promote MICP: 1) microbial cultures provided a source of the urease enzyme to catalyze ureolysis and a biofilm template for mineral nucleation and 2) urea-calcium media promoted supersaturated conditions favoring precipitation of calcium carbonate. Overnight cell cultures of *S. pasteurii* (ATCC11859) were started from frozen stocks in 18.5 g/L Brain Heart Infusion (BHI, Becton Dickinson, Franklin Lakes, NJ) media plus 2% urea in flasks placed in a 30°C incubating shaker. These overnight cultures varied in volume from 150 – 500 mL, with most being 300 mL. The overnight cultures were added directly to fresh yeast extract-based nutrient solution (YE-) consisting of 15.5 g/L yeast extract (Acros Organics, Geel, Belgium), 24 g/L urea (Dyno Nobel, Inc, Deer Island OR), and 1 g/L NH_4Cl (BASF USA, Florham Park, NJ) for a final volume of 15 L and mixed on a stir plate for approximately 24 hours prior to injection. During the second half of the experiment, some 15 L cultures were also inoculated with previous batches of inocula. Supplemental aeration was provided by aquarium air pumps (Aqua Culture MK-1504 and Topfin AIR-2000) fitted with 5-inch bubble diffusers (Aqua Culture, Walmart). The 15 L inoculum cultures were heated by seed heating mats wrapped around the carboy and by heating the mobile laboratory trailer to approximately 75 – 80 °F. Inocula injected on Day 6 were amended with 50 – 200 g Jack Bean meal (Sigma-Aldrich, St. Louis, MO), a plant-based source of the urease enzyme, and 100-250 g urea per 15 L batch immediately prior to filling the bailer to augment urea hydrolysis in the treatment zone. Before filling the bailer for an injection, the pH and electrical conductivity (EC) of the cultures were measured. Samples were collected for urea analysis with the Jung Assay (Jung *et al*., 1975), population analysis using the drop plate method (Herigstad *et al*., 2001), and optical density (OD 600).

Calcium media (YE+) (125 g/L $CaCl_2*2H_2O$ (Peladow, Occidental Chemical Corp., Dallas, TX), 72 g/L urea, 3 g/L NH_4Cl and 9 g/L yeast extract) was mixed several hours prior to injection in 15 L batches. Each batch was mixed with a drill-powered mixer and sampled for pH, urea, and Ca^{2+} prior to filling the bailer.

Recent laboratory studies have suggested that more frequent inoculation, or stimulation of bacterial growth with nutrient solution, improves the efficiency of ureolysis-driven calcite precipitation (Kirkland *et al*., 2019). Therefore, a cycle of one inoculum injection followed by two calcium media injections was applied. The field demonstration design included 3 – 4 such cycles during a work-day at the field site.

2.4 Experiment termination and post-experiment analysis

The demonstration was concluded on Day 6 due to approaching inclement weather which would have created hazardous conditions at the wellhead. The crane, slickline truck, and mobile laboratory were removed from the site. There was no activity in the well for approximately 2 weeks. Then a post-MICP treatment injection test was conducted, a temperature log was acquired, and the tubing string was removed from the well.

Accumulated mineral material not present during the placement of the 2-7/8 inch (7.3 cm) tubing string was scraped from the perforated pup joint following removal of the tubing string from the well. Approximately 50 g of the mineral material was sampled for analysis at MSU. Some of the material was pulverized for analysis with XRD; some was digested with acid to

quantify calcium content, while other samples of the material were imaged using FE-SEM and confocal microscopy. DNA was also extracted for sequencing from both the solid mineral and from a liquid enrichment inoculated with the mineral. The specific methods are described in more detail below.

Sub-samples of the pup joint mineral material were crushed, dried, and weighed before being subjected to digestion in 10% trace metal grade nitric acid to dissolve the mineral components. The digestate was analyzed with a colorimetric assay to quantify the calcium content (Phillips, 2013). Sub-samples of the pup joint mineral material were also dried, pulverized with a mortar and pestle, and lightly sprinkled onto a glass slide coated with a thin layer of petroleum jelly for analysis with a Scintag X1 Powder X-ray diffractometer (XRD) and a Cu k-alpha X-ray source.

Sub-samples from both the outer surface and the inner region of the pup joint mineral material were dried and crushed prior to FE-SEM imaging. Sub-samples mounted for micro-imaging were sputter-coated with Ir for 1 minute at 20 mA. High resolution micrographs were collected on a Zeiss Supra 55VP field emission scanning electron microscope at 1.0 kV and a working distance of 3 – 5 mm.

An outer surface sub-sample of the mineral material was prepared for confocal microscopy by staining with 1 µL SYBR Green I nucleic acid stain in 1 mL Milli-Q deionized water for 1 hour in the dark. After staining, the sub-sample was rinsed with Milli-Q water and imaged using a 488 nm laser using an upright Leica SP5 confocal scanning laser microscope (CSLM). Images were processed for qualitative analysis using Imaris software (Bitplane, Zurich, Switzerland).

A small piece of the mineral material, approximately 2 g, was placed in a 500 mL media bottle containing 150 mL sterile CMM- media (3 g/L Difco Nutrient Broth, 20 g/L urea, 10 g/L NH_4Cl) to culture potential ureolytic microbes entrained in the mineral. The bottle was placed on a shaker table at 150 rpm at room temperature for 2 weeks. DNA was extracted from the liquid enrichment and also from an untreated 500mg sample of the mineral material using the MP Biomedicals FastDNA™ Spin kit for soil along with the MP Biomedicals FastPrep®-24 bead beater. Extracted DNA concentrations were determined with an invitrogen™ Qubit® fluorometer. q-PCR and 16S rRNA gene sequencing was performed on both samples as described in the Supporting Information of (Phillips *et al.*, 2016). Samples from the liquid enrichment were plated on BHI agar plates amended with 2% urea to isolate predominant microbes. Four of the isolates were identified with 16S rRNA gene sequencing and cultured for batch studies to assess their ureolytic activity.

3. Results and Discussion

3.1 Reduced Injectivity

The flow-to-pressure ratio [gpm/psi] is an indication of the ease with which fluids can move through fractures, cement defects, or the pore space of a rock formation; a lower value implies lower permeability and limited injectivity. To improve readability, we will refer to this flow-to-pressure ratio hereafter as injectivity. After 25 inoculum injections (approximately 95 gal. (360 L)) and 49 calcium media injections (185 gal (700 L)), the injectivity of the system had decreased from 10.4×10^{-3} gpm/psi (5.7 L/min/MPa) to 3×10^{-3} gpm/psi (1.6 L/min/MPa), a reduction of approximately 70% (Figure 4). During the first two days, the total volume of water injected after each bailer and actual pumping flow rates were recorded only periodically.

Subsequently, pumping flow rates were recorded for each bailer run (Supporting Information). On Day 4, several failed bailer dumps, shown as open markers in Figure 4, were followed by an increase in injectivity. In these instances, water pumped down the tubing to push the bailer contents into the formation only further diluted the reactants in the cement defect and rock matrix since the bailer failed to release its contents. The cause of the pressure loss is unknown, though possible explanations include breakthrough of a thin MICP biomineral seal, a new fracture in the wellbore cement, or expansion of flow to higher portions of the sandstone thief zone. The injectivity again decreased on Days 5 and 6 after the Day 4 increase. Pumping tests conducted approximately two weeks after the end of the field experiment yielded an injectivity consistent with those recorded at the end of Day 6. The injection consisted of an additional 1,890 gallons (7,154 L) of water delivered at 2.25 gpm (8.5 L/min) and a pressure of 740.5 psi (5.1 MPa). The injectivity of the final injection was 0.003 gpm/psi (1.6 L/min/MPa). These data indicate that the MICP biomineral was stable over the two-week injection hiatus and that no significant additional reduction in injectivity occurred after the end of the field demonstration.

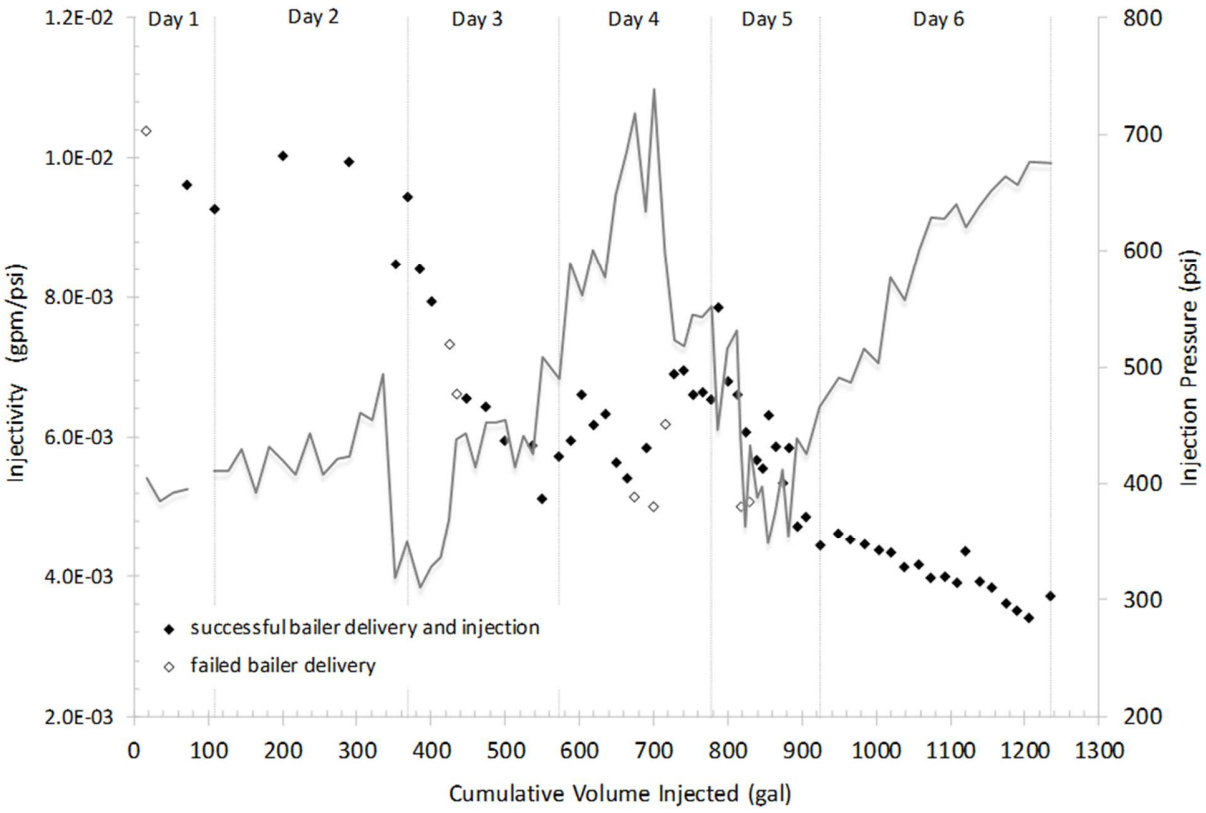

Figure 4. The flow-to-pressure ratio, or injectivity, declined by 70% after six days of injection of biomineralization-promoting fluids. Open markers indicate injections when the bailer delivering the fluids downhole failed to open and release the mineralization-promoting fluids. The solid line is a modified form of the Hall plot, showing changes in injection pressure with respect to volume of fluids injected. Vertical lines mark the days of the experiment. The final injection, 2 weeks after the end of the experiment, is not shown due to scale. The injection consisted of an additional 1,890 gallons (7,154 L) of water delivered at

2.25 gpm (8.5 L/min) at a pressure of 740.5 psi (5.1 MPa). The injectivity of the final injection was 0.003 gpm/psi (1.6 L/min/MPa).

Also shown in Figure 4 is a modified form of the Hall plot (Izgec *et al.*, 2009, 2011) wherein the cumulative volume of fluids injected is plotted against injection pressure. Injection pressure generally increases with the volume of mineralization-promoting fluids injected, as expected. The decrease in pressure which appears between 335 – 350 gal (1268 – 1325 L) and 700 – 850 gal (2650 – 3218 L) is an indication that the injection flow rate was reduced to avoid over-pressurization. This view of the data also appears to corroborate the hypothesis that the increase in injectivity observed Day 4 may have resulted from elevated injection pressures on Day 4.

3.2 Post-experimental well characterization

Temperature logs were acquired over the zone of interest before and after the MICP treatment, with 30-minute intervals between passes of the instrument. Spacing of the lines indicates the rate at which the temperature recovers following injection of a colder fluid. More closely spaced lines indicate slower temperature recovery caused by higher volumes of cold water reaching the area. More widely spaced lines suggest that less water was injected into the region and temperature variation is dominated by the thermal gradient of the well. Relative to the temperature log conducted before the MICP treatment (Figure 5, left), the post-MICP temperature log shows more widely spaced temperature values between the passes of the instrument (Figure 5, right). Comparison of these two temperature logs provides evidence that significantly less water traveled into the channel above 2280 ft (695 m) bgs. There is little evidence of influence from the cooler fluids above 2230 ft (684.5 m) bgs. The post-demonstration temperature log suggests MICP treatment partially sealed the leakage pathway to the thief zone and provides validation of the conceptual model explaining the change in injectivity and mode of well failure.

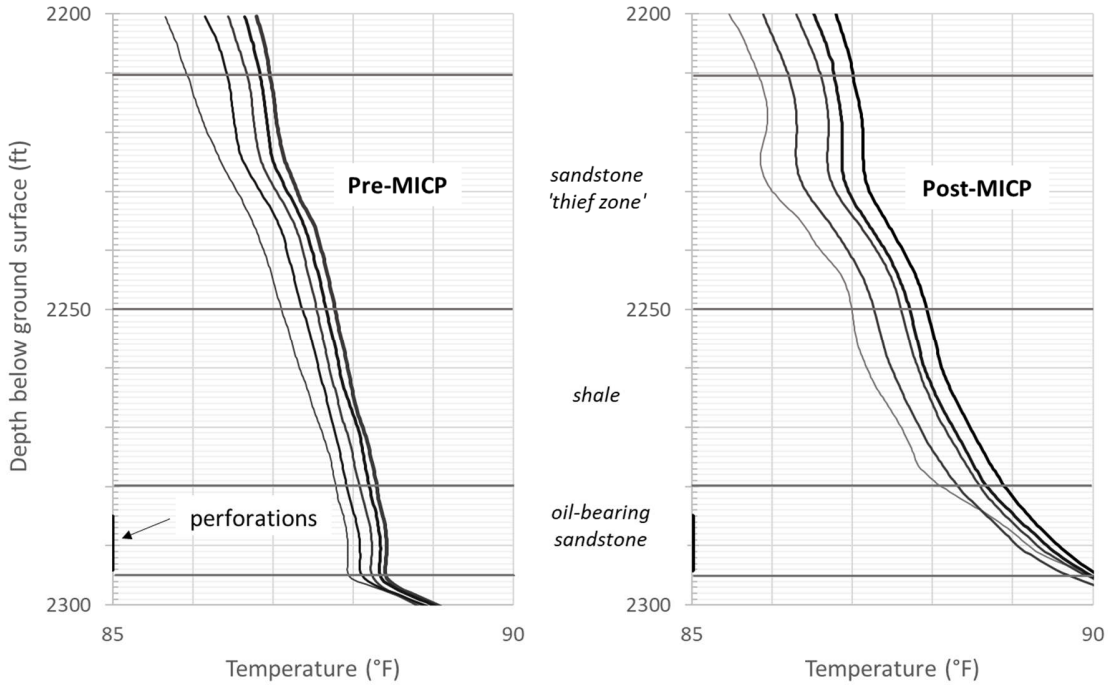

Figure 5. Temperature logs collected pre-MICP (left) show closer spacing of the temperature log lines indicating fluid flow through a channel between the perforated zone (black bar) in the target oil-bearing sandstone and the thief zone. Post-MICP (right) shows reduced fluid flow through the region of the channel after treatment, indicated by the wider spacing of the measurement passes.

3.4 Mineral precipitate analysis

The outer surface of the mineral precipitate that formed on the perforated pup joint where the bailer dumped the biomineralization-promoting fluids was coated in a black substance while the inner layers were lighter colored and grainy in appearance (Figure 6). This material was not present when the tubing string was deployed in the well prior to the field demonstration. It is likely that the mineral material accumulated over the course of the field demonstration due to the injection of MICP-promoting fluids.

Figure 6. Mineral precipitation was observed on the downhole tubing following completion of the field demonstration, visible as the bumpy coating on the perforated pup joint (left). The outer surface was darker in color than the inner regions of the precipitate (right), perhaps due to exposure to wellbore fluids following the field demonstration.

Calcium assays of two samples of the mineral showed that calcium ion composed on average 39.6% of the sample mass, consistent with gravimetric measurements that indicate calcium accounted for 37.7% of the sample mass. By stoichiometry, calcium could be a maximum of 40% of digested $CaCO_3$ mass. XRD results for two sub-samples of the pup joint mineral indicate that the mineral consists entirely of calcite ($CaCO_3$) (Supporting Information).

FE-SEM images of the pup joint mineral sample show crystal structures consistent with calcite minerals as well as round vaterite-like forms (Figure 7) and amorphous deposits. No cells were readily apparent in the FE-SEM micrographs, even after lightly washing the samples in a 1% HCl solution to dissolve the top layer of mineral. Chemical and microscopy analyses of the mineral material removed from the pup joint confirm the material to be calcium carbonate, as would be expected following the injection of MICP-promoting fluids.

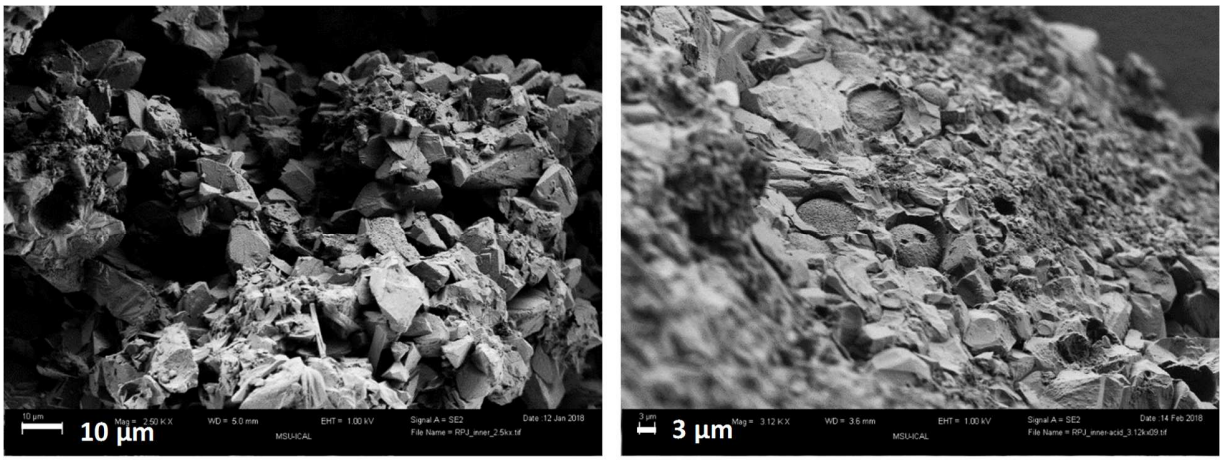

Figure 7. FE-SEM image of the mineral scale which accumulated on the surface of the pup joint downhole in the subject well after rinsing with 1% HCl solution. Material collected from the inner region of the scale shows angular crystals consistent with calcite and amorphous mineral forms (left) while the outer region of the mineral scale also includes examples of a round crystal morphology that is consistent with vaterite (right).

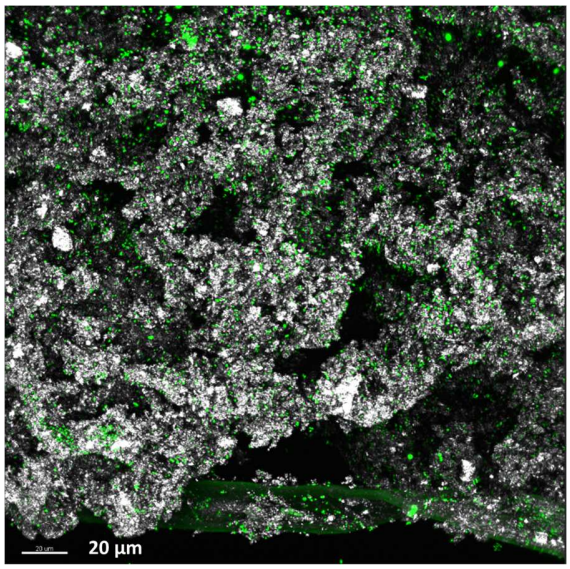

Figure 8. A 2D projection of a combined reflection and fluorescent image from the confocal microscope shows cells (SYBR Green I) in association with mineral precipitation. Scale bar is 20 µm. Image by Sobia Anjum, image analysis by Betsey Pitts.

Although no cells were observed during FE-SEM imaging, the confocal images revealed a dense microbial population associated with the precipitate, as would be expected with MICP. The 2D projection of combined reflection and fluorescent confocal images of the mineral is shown in Figure 8. The green flecks, labeled with SYBR-Green I nucleic acid stain, are likely bacteria though DNA-containing cell fragments could fluoresce as well. Since no attempt was made to use aseptic sampling methods, the microbes present may have been introduced at any time, including after the tubing string was removed from the well though samples were taken as quickly as possible. Further microbiological analysis methods were applied to identify organisms that could have participated in the MICP process.

DNA was extracted both from the solid mineral and from a liquid enrichment. More microbial diversity was observed from the solid sample where the genus of bacterium injected, *Sporosarcina*, made up only 0.3% of the microbial community. In the enrichment, *Sporosarcina spp.* accounted for 41% of the community (Figure 9). This result is not unusual since the nutrient solution used in the enrichment is designed to culture ureolytic microbes. Isolations of microbes from the enrichment culture identified three organisms - *Sporosarcina pasteurii,* a *Shewanella* sp.*,* and a *Sphingobacterium sp.* – that were capable of hydrolyzing urea in subsequent batch activity studies. This suggests that native ureolytic species of microbes may have been stimulated by the injections of nutrient solution and may have participated in the MICP process during the field demonstration.

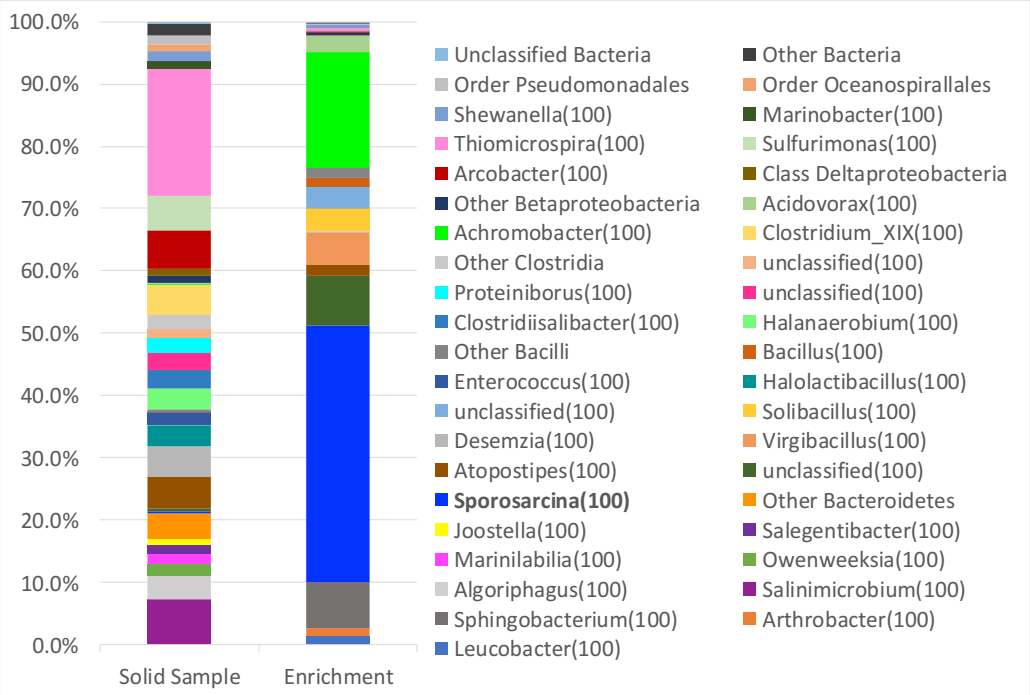

Figure 9. The microbial community extracted from the carbonate mineral itself resulted in a rich diversity with only a small percentage (0.3%) of the population identified as *Sporosarcina spp.*, the injected microorganism. In contrast, in the liquid sample that was enriched in the laboratory *Sporosarcina* spp. were dominant making up 41% of the population. (Chiachi Hwang)

4. Conclusions

This field demonstration used injections of MICP-promoting fluids in a water injection well with the intent to 1) validate a conceptual model of wellbore cement failure derived from analysis of well logs and injectivity data and 2) provide proof of principle that MICP can reduce system permeability in the presence of oil and using conventional oilfield fluid delivery methods. Pressure and flow rate were monitored during the MICP injections, revealing a 70% decrease in injectivity over the course of the demonstration. A post-treatment overnight injection test with a final rate of 2.25 gpm at 740.5 psia indicated the injectivity was stable two weeks after the end of the experiment. The post-treatment temperature log showed the majority of the injectate staying contained in an area within a few feet of the perforations, indicating that flow through the cement defect to the thief zone was significantly curtailed. When the MICP injection tubing was removed from the well there was considerable calcite precipitation apparent on the perforated pipe sections. Mineralogical and microbiological analyses of the mineral removed from the injection tubing confirm that MICP can occur downhole in the presence of oil.

The volume of calcium carbonate that formed in undesirable flow paths in the wellbore cement channel and sandstone thief zone was sufficient to reduce the leakage pathway but did not restore the historic injection flow-to-pressure relationship of approximately 1 gpm at 1400 psi (3.8 L/min at 9.7 MPa). In the authors' opinion, the most likely explanation is related to the volume of the void space to be filled by $CaCO_3$ precipitation relative to the ability of the bailer to deliver adequate volumes of microbes and calcium media in the timeframe allotted for the

demonstration. A subsequent field demonstration has been planned in the same well where larger volumes of reactants will be injected in an attempt to restore the historic injection flow-to-pressure relationship.

The work presented here shows that common well logs, including sonic, ultrasonic, and temperature logs, can be used to identify scenarios where MICP can be employed using conventional methods to reduce system permeability, remediate leakage pathways, and improve waterflood efficiency. Furthermore, this study verifies that the MICP biochemical reaction can occur in the presence of hydrocarbons.

Acknowledgements

This material is based upon work supported by the Department of Energy under Grant No. DE-FE0024296. Any opinions, findings, conclusions or recommendations expressed herein are those of the authors and do not necessarily reflect the views of the Department of Energy (DOE). This work was performed in part at the Montana Nanotechnology Facility (MONT), a member of the National Nanotechnology Coordinated Infrastructure (NNCI), which is supported by the National Science Foundation (Grant# ECCS-1542210). The authors thank Laura Dobeck, Chiachi Hwang, Sobia Anjum, Neerja Zambare, Zach Frieling, Paige Tunby, and Betsey Pitts at the Center for Biofilm Engineering and Nathaniel Rieders at the Image and Chemical Analysis Laboratory (ICAL) at Montana State University.

Author Information

Corresponding Authors:
Catherine M Kirkland catherine.kirkland@montana.edu
Adrienne J Phillips adrienne.phillips@montana.edu
Center for Biofilm Engineering
Montana State University
366 Barnard Hall
Bozeman, MT 59717

References

Ahmed, A. A. and Mohamed, A. P. I., 2015 In-depth permeability modifier for improvement of sweep efficiency in a heterogeneous oil reservoir: A review. *Research Journal of Applied Sciences, Engineering and Technology*, **9**(1),18-28. https://doi.org/10.19026/rjaset.9.1371

Bai, M. X., Zhang, Z. C. and Fu, X. F., 2016 A review on well integrity issues for co2 geological storage and enhanced gas recovery. *Renewable & Sustainable Energy Reviews*, **59**(920-926. https://doi.org/10.1016/j.rser.2016.01.043

Burbank, M. B., Weaver, T. J., Green, T. L., Williams, B. C. and Crawford, R. L., 2011 Precipitation of calcite by indigenous microorganisms to strengthen liquefiable soils. *Geomicrobiology Journal*, **28**(4),301-312. https://doi.org/10.1080/01490451.2010.499929

Carroll, S. A., Iyer, J. and Walsh, S. D. C., 2017 Influence of chemical, mechanical, and transport processes on wellbore leakage from geologic co2 storage reservoirs. *Accounts of Chemical Research*, **50**(8),1829-1837. https://doi.org/10.1021/acs.accounts.7b00094

Cuthbert, M. O., McMillan, L. A., Handley-Sidhu, S., Riley, M. S., Tobler, D. J. and Phoenix, V. R., 2013 A field and modeling study of fractured rock permeability reduction using microbially induced

calcite precipitation. *Environmental Science & Technology*, **47**(23),13637-13643. https://doi.org/10.1021/es402601g

Davies, R. J., Almond, S., Ward, R. S., Jackson, R. B., Adams, C., Worrall, F., Herringshaw, L. G., Gluyas, J. G. and Whitehead, M. A., 2014 Oil and gas wells and their integrity: Implications for shale and unconventional resource exploitation. *Marine and Petroleum Geology*, **56**(239-254. https://doi.org/10.1016/j.marpetgeo.2014.03.001

De Andrade, J. and Sangesland, S., 2016 Cement sheath failure mechanisms: Numerical estimates to design for long-term well integrity. *Journal of Petroleum Science and Engineering*, **147**(682-698. https://doi.org/10.1016/j.petrol.2016.08.032

Decho, A. W., 2010 Overview of biopolymer-induced mineralization: What goes on in biofilms? *Ecological Engineering*, **36**(2),137-144. https://doi.org/10.1016/j.ecoleng.2009.01.003

Feng, Q., Wang, S., Zhang, W., Song, Y. and Song, S., 2013 Characterization of high-permeability streak in mature waterflooding reservoirs using pressure transient analysis. *Journal of Petroleum Science and Engineering*, **110**(55-65. https://doi.org/10.1016/j.petrol.2013.08.042

Ferris, F. G., Phoenix, V., Fujita, Y. and Smith, R. W., 2003 Kinetics of calcite precipitation induced by ureolytic bacteria at 10 to 20 degrees c in artificial groundwater. *Geochimica et Cosmochimica Acta*, **67**(8),1701-1722. https://doi.org/10.1016/s0016-7037(00)00503-9

Ferris, F. G., Stehmeier, L. G., Kantzas, A. and Mourits, F. M., 1996 Bacteriogenic mineral plugging. *Journal of Canadian Petroleum Technology*, **35**(8),56-61. https://doi.org/10.2118/96-08-06

Fridjonsson, E. O., Seymour, J. D., Schultz, L. N., Gerlach, R., Cunningham, A. B. and Codd, S. L., 2011 Nmr measurement of hydrodynamic dispersion in porous media subject to biofilm mediated precipitation reactions. *Journal of Contaminant Hydrology*, **120-21**(79-88. https://doi.org/10.1016/j.jconhyd.2010.07.009

Fujita, Y., Taylor, J. L., Gresham, T. L. T., Delwiche, M. E., Colwell, F. S., McLing, T. L., Petzke, L. M. and Smith, R. W., 2008 Stimulation of microbial urea hydrolysis in groundwater to enhance calcite precipitation. *Environmental Science & Technology*, **42**(8),3025-3032. https://doi.org/10.1021/es702643g

Gomez, M. G., Martinez, B. C., DeJong, J. T., Hunt, C. E., deVlaming, L. A., Major, D. W. and Dworatzek, S. M., 2015 Field-scale bio-cementation tests to improve sands. *Proceedings of the Institution of Civil Engineers-Ground Improvement*, **168**(3),206-216. https://doi.org/10.1680/grim.13.00052

Haagsma, A., Weber, S., Moody, M., Sminchak, J., Gerst, J. and Gupta, N., 2017 Comparative wellbore integrity evaluation across a complex of oil and gas fields within the michigan basin and implications for co2 storage. *Greenhouse Gases-Science and Technology*, **7**(5),828-842. https://doi.org/10.1002/ghg.1620

Herigstad, B., Hamilton, M. and Heersink, J., 2001 How to optimize the drop plate method for enumerating bacteria. *Journal of Microbiological Methods*, **44**(2),121-129. https://doi.org/http://dx.doi.org/10.1016/S0167-7012(00)00241-4

Ingraffea, A. R., Wells, M. T., Santoro, R. L. and Shonkoff, S. B. C., 2014 Assessment and risk analysis of casing and cement impairment in oil and gas wells in pennsylvania, 2000–2012. *Proceedings of the National Academy of Sciences*, **111**(30),10955-10960. https://doi.org/10.1073/pnas.1323422111

Izgec, B. and Kabir, S., 2009 Real-time performance analysis of water-injection wells. *SPE Reservoir Evaluation & Engineering - SPE RESERV EVAL ENG*, **12**(116-123. https://doi.org/10.2118/109876-PA

Izgec, B. and Kabir, S., 2011 Identification and characterization of high-conductive layers in waterfloods. *SPE Reservoir Evaluation & Engineering*, **14**(01),113-119. https://doi.org/10.2118/123930-PA

Johns, J. E., Blount, C. G., Dethlefs, J. C., Loveland, M. J., McConnell, M. L., Schwartz, G. L. and Julian, J. Y., 2009 Applied ultrasonic technology in wellbore-leak detection and case histories in alaska

606 north slope wells. *Spe Production & Operations*, **24**(2),225-232. https://doi.org/10.2118/102815-
607 pa
608 Jung, D., Biggs, H., Erikson, J. and Ledyard, P. U., 1975 New colorimetric reaction for endpoint,
609 continuous-flow and kinetic measurement of urea *Clinical Chemistry*, **21**(8),1136-1140.
610 Kargozarfard, Z., Riazi, M. and Ayatollahi, S., 2019 Viscous fingering and its effect on areal sweep
611 efficiency during waterflooding: An experimental study. *Petroleum Science*, **16**(1),105-116.
612 https://doi.org/10.1007/s12182-018-0258-6
613 Kirkland, C. M., Norton, D., Firth, O., Eldring, J., Cunningham, A. B., Gerlach, R. and Phillips, A. J., 2019
614 Visualizing micp with x-ray uct to enhance cement defect sealing. *International Journal of*
615 *Greenhouse Gas Control*, **86**(93 - 100 https://doi.org/10.1016/j.ijggc.2019.04.019
616 Newell, D. L. and Carey, J. W., 2013 Experimental evaluation of wellbore integrity along the cement-rock
617 boundary. *Environmental Science & Technology*, **47**(1),276-282.
618 https://doi.org/10.1021/es3011404
619 Opedal, N. V., Torsaeter, M., Vralstad, T. and Cerasi, P., 2014 Potential leakage paths along cement-
620 formation interfaces in wellbores; implications for co2 storage. *7th Trondheim Conference on*
621 *Co2 Capture, Transport and Storage (2013)*, **51**(56-64.
622 https://doi.org/10.1016/j.egypro.2014.07.007
623 Oppenheimer-Shaanan, Y., Sibony-Nevo, O., Bloom-Ackermann, Z., Suissa, R., Steinberg, N.,
624 Kartvelishvily, E., Brumfeld, V. and Kolodkin-Gal, I., 2016 Spatio-temporal assembly of functional
625 mineral scaffolds within microbial biofilms. *Npj Biofilms and Microbiomes*,
626 **2**(https://doi.org/10.1038/npjbiofilms.2015.31
627 Phillips, A. J., Cunningham, A. B., Gerlach, R., Hiebert, R., Hwang, C., Lomans, B. P., Westrich, J., Mantilla,
628 C., Kirksey, J., Esposito, R. and Spangler, L., 2016 Fracture sealing with microbially-induced
629 calcium carbonate precipitation: A field study. *Environmental Science & Technology*, **50**(7),4111-
630 4117. https://doi.org/10.1021/acs.est.5b05559
631 Phillips, A. J., Gerlach, R., Lauchnor, E., Mitchell, A. C., Cunningham, A. B. and Spangler, L., 2013
632 Engineered applications of ureolytic biomineralization: A review. *Biofouling*, **29**(6),715-733.
633 https://doi.org/10.1080/08927014.2013.796550
634 Phillips, A. J., Lauchnor, E., Eldring, J., Esposito, R., Mitchell, A. C., Gerlach, R., Cunningham, A. B. and
635 Spangler, L. H., 2013 Potential co2 leakage reduction through biofilm-induced calcium carbonate
636 precipitation. *Environmental Science & Technology*, **47**(1),142-149.
637 https://doi.org/10.1021/es301294q
638 Phillips, A. J., Troyer, E., Hiebert, R., Kirkland, C. M., Gerlach, R., Cunningham, A., Spangler, L., Kirksey, J.,
639 Rowe, W. and Esposito, R., 2018 Enhancing wellbore cement integrity with microbially induced
640 calcite precipitation (micp): A field scale demonstration. *Journal of Petroleum Science and*
641 *Engineering*, **171**(1141-1148. https://doi.org/10.1016/j.petrol.2018.08.012
642 Stocks-Fischer, S., Galinat, J. K. and Bang, S. S., 1999 Microbiological precipitation of caco3. *Soil Biology*
643 *and Biochemistry*, **31**(11),1563-1571. https://doi.org/10.1016/s0038-0717(99)00082-6
644 Todorovic, J., Raphaug, M., Lindeberg, E., Vralstad, T. and Buddensiek, M. L., 2016 Remediation of
645 leakage through annular cement using a polymer resin: A laboratory study. *8th Trondheim*
646 *Conference on Co2 Capture, Transport and Storage*, **86**(442-449.
647 https://doi.org/10.1016/j.egypro.2016.01.045
648 Udy, J., Hansen, B., Maddux, S., Petersen, D., Heilner, S., Stevens, K., Lignell, D. and Hedengren, J. D.,
649 2017 Review of field development optimization of waterflooding, eor, and well placement
650 focusing on history matching and optimization algorithms. *Processes*,
651 **5**(3),https://doi.org/10.3390/pr5030034

van Paassen Leon, A., Ghose, R., van der Linden, T. J. M., van der Star, W. R. L. and van Loosdrecht, M. C. M., 2010 Quantifying biomediated ground improvement by ureolysis: Large-scale biogrout experiment. *Journal of Geotechnical and Geoenvironmental Engineering*, **136**(12),1721-1728.

Verba, C., Thurber, A. R., Alleau, Y., Koley, D., Colwell, F. and Torres, M. E., 2016 Mineral changes in cement-sandstone matrices induced by biocementation. *International Journal of Greenhouse Gas Control*, **49**(312-322. https://doi.org/10.1016/j.ijggc.2016.03.019

Wang, W. and Taleghani, A. D., 2014 Three-dimensional analysis of cement sheath integrity around wellbores. *Journal of Petroleum Science and Engineering*, **121**(38-51. https://doi.org/10.1016/j.petrol.2014.05.024

Wu, J., Wang, X.-B., Wang, H.-F. and Zeng, R. J., 2017 Microbially induced calcium carbonate precipitation driven by ureolysis to enhance oil recovery. *RSC Advances*, **7**(59),37382-37391. https://doi.org/10.1039/C7RA05748B

Yuan, B. and Wood, D. A., 2018 A comprehensive review of formation damage during enhanced oil recovery. *Journal of Petroleum Science and Engineering*, **167**(287-299. https://doi.org/https://doi.org/10.1016/j.petrol.2018.04.018

Zimmerman, R. W. and Bodvarsson, G. S., 1996 Hydraulic conductivity of rock fractures. *Transport in Porous Media*, **23**(1),1-30.